*Journal of Fluids and Structures* (2000) **14,** 697–709
doi:10.1006/jfls.2000.0290 available online at http://www.idealibrary.com on IDEAL®

# GROUND EFFECT OF FLOW AROUND AN ELLIPTIC CYLINDER IN A TURBULENT BOUNDARY LAYER

J.-H. Choi and S.-J. Lee

*Department of Mechanical Engineering, Pohang University of Science & Technology Pohang, Korea*

(Received 10 February 1999, and in final form 10 January 2000)

The flow characteristics around an elliptic cylinder with an axis ratio of AR = 2 located near a flat plate were investigated experimentally. The elliptic cylinder was embedded in a turbulent boundary layer whose thickness is larger than the cylinder height. For comparison, the same experiment was carried out for a circular cylinder having the same vertical height. The Reynolds number based on the height of the cylinder cross-section was 14000. The pressure distributions on the cylinder surface and on the flat plate were measured for various gap distances between the cylinder and the plate. The wake velocity profiles behind the cylinder were measured using hot-wire anemometry. In the near-wake region, the vortices are shed regularly only when the gap ratio is greater than the critical value of $G/B = 0{\cdot}4$. The critical gap ratio is larger than that of a circular cylinder. The variation of surface pressure distributions on the elliptic cylinder with respect to the gap ratio is much smaller than that on the circular cylinder. This trend is more evident on the upper surface than the lower one. The surface pressures on the flat plate recover faster than those for the case of the circular cylinder at downstream locations. As the gap ratio increases, the drag coefficient of the cylinder itself increases, but the lift coefficient decreases. For all gap ratios tested in this study, the drag coefficient of the elliptic cylinder is about half that of the circular cylinder. The ground effect of the cylinder at small gap ratio constrains the flow passing through the gap, and restricts the vortex shedding from the cylinder, especially in the lower side of the cylinder wake. This constraint effect is more severe for the elliptic cylinder, compared to the circular cylinder. The wake region behind the elliptic cylinder is relatively small and the velocity profiles tend to approach rapidly to those of a flat plate boundary layer


## 1. INTRODUCTION

Flow around bluff bodies has been widely investigated for their own academic interest as well as wide practical applications. Especially, the wake behind a circular cylinder has been studied numerically and experimentally by many investigators due to its periodic vortex shedding and simple geometry. As an extension, the flow around a circular cylinder located near a flat plate is an interesting topic to be investigated. This kind of study can be applied to many engineering problems such as undersea pipelines, building constructions and heat transfer enhancement of heat exchangers.

The interaction between the boundary layer developed over a flat plate and the cylinder wake has been studied from the following two viewpoints. The first is to study the effect of the presence of a cylinder in the turbulent boundary layer over a flat surface, where the cylinder controls the turbulent boundary layer flow. The second viewpoint is to study the effect of the boundary layer profiles on the flow around the cylinder.

Marumo *et al.* (1978) investigated the boundary layer disturbed by a cylinder for various gap ratios. From this study, the boundary layer was found to recover faster at the inner

0889–9746/00/070697 + 14 $35.00/0 

(near the plate) region than the outer region. In addition, the velocity fluctuations were recovered faster than the mean velocity components.

Bearman & Zdravkovich (1978) measured pressure distribution and vortex shedding for various gaps of a circular cylinder embedded in a boundary layer whose thickness was 0·8 times the cylinder diameter. They found that the vortex shedding was restricted for small gaps less than the critical gap ratio of 0·3 and the Strouhal number St was nearly constant for gap ratios greater than the critical value.

Angrilli & Bergamaschi (1982) investigated the wall effect on vortex-shedding frequency at low subcritical Reynolds numbers, where the boundary layer thickness was 0·25 times the cylinder diameter. They found, however, that the vortex-shedding frequency increases as the cylinder approaches the wall. Taniguchi & Miyakoshi (1990) measured the fluctuating fluid forces and pressure distributions acting on a circular cylinder located near a plane wall to study the effect of boundary layer thickness on the critical gap ratio. They revealed that the Strouhal number was about 0·2 and almost independent of the boundary layer thickness.

In most previous studies, a circular cylinder was immersed in a relatively thin boundary layer, whereas the case where the boundary layer thickness is much greater than the cylinder diameter has received relatively little attention. In addition, noncircular cylinders such as elliptic and rectangular cylinders are sometimes preferred, rather than the circular cylinder, for special applications. For example, the drag coefficient of elliptic cylinders at a small angle of attack is much smaller than that of a circular cylinder in aerodynamic applications. The heat transfer coefficient of elliptic cylinders was also found to be nearly equal to or a little higher than that of a circular cylinder (Ota *et al.* 1984, 1987). Furthermore, elliptic cylinders have the general fluid dynamic features between those of a circular cylinder (AR = 1) and a flat plate (AR = $\infty$). Flow characteristics of the wake behind elliptic cylinders located in a uniform flow are changed considerably depending on the angle of attack and the axis ratio (AR) of the cylinder (Modi & Wiland 1970; Modi & Dikshit 1975). The elliptic cylinder has wide engineering applications and can be used as an effective passive tool to control the flow nearby.

However, as far as we know, there was no study published in the literature on the interaction between an elliptic cylinder placed near a flat plate and the turbulent boundary layer. In this study, the ground effect on the flow characteristics around an elliptic cylinder immersed in a thick turbulent boundary layer has been investigated experimentally for various gap ratios.

## 2. EXPERIMENTAL APPARATUS AND METHODS

Experiments were performed in a closed return wind tunnel with a test-section of 0·6 m in height, 0·72 m in width and 6 m in length. The free-stream turbulent intensity in the test-section was less than 0·08% at 10 m/s.

Figure 1 shows the geometric shape of cylinder models used in this study and the schematic diagram of the experimental set-up. An elliptic cylinder having an axis ratio (AR = $A/B$) of 2 was used in this study, where $A$ and $B$ are radii of the major and minor axes of the elliptic cylinder. For comparison, the same experiment was carried out for a circular cylinder having the same height as the cylinder cross-section. The diameter and aspect ratio ($L/D$) of the circular cylinder (AR = 1) are $D$ = 21·2 mm and 28·3, respectively.

A smooth flat plate 15 mm in thickness and 4·8 m in length was installed 100 mm above the bottom surface of the test-section. The leading edge of the plate was sharp-edged with an angle of 30°. The elliptic cylinder was located at 1·5 m downstream from the leading edge of the flat plate. A trip wire of 3·5 mm diameter was attached on the plate surface at 100 mm downstream from the leading edge to generate a thick turbulent boundary layer. The

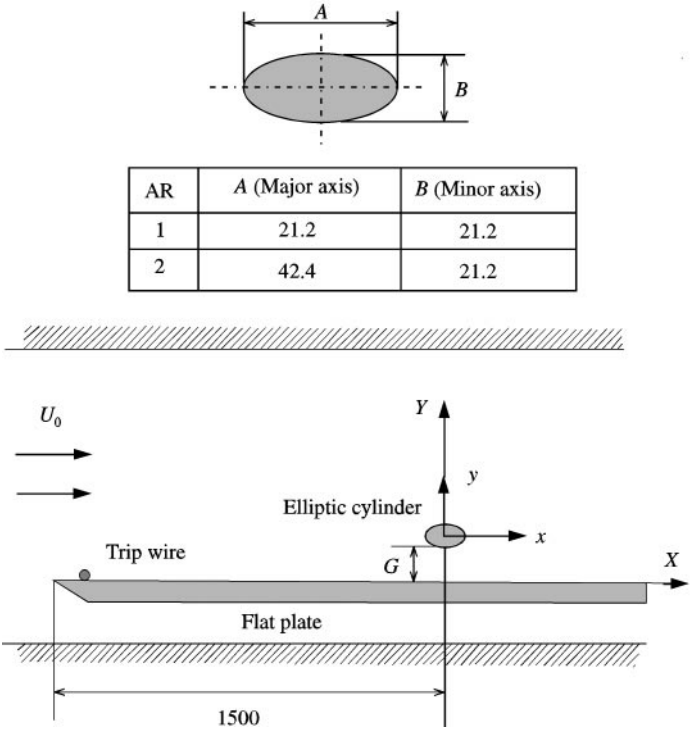


| AR | A (Major axis) | B (Minor axis) |
|---|---|---|
| 1 | 21.2 | 21.2 |
| 2 | 42.4 | 21.2 |

Figure 1. Geometric shape of elliptic cylinders and schematic diagram of experimental set-up (dimensions: mm).

boundary layer formed over the flat plane has a thickness of 75 mm at the cylinder location. At the two ends of the elliptic cylinder spanning the wind tunnel test-section, rectangular end-plates were attached to maintain the two-dimensional characteristics of the cylinder wake by minimizing the effect of the boundary layer developed along the wind tunnel side-walls. During experiments, the free-stream velocity ($U_0$) was fixed at 10 m/s and the corresponding Reynolds number based on the height of the cylinder cross-section was about $1{\cdot}4 \times 10^4$.

The coordinates $X$ and $Y$ denote the streamwise distance from the cylinder and the vertical distance from the bottom plate, respectively. The coordinates $x$ and $y$ indicate the corresponding relative distances from the centre of the cylinder; $G$ represents the gap distance between the bottom of the cylinder and the flat plate.

To measure the pressure distributions on the cylinder surface and on the flat plate, pressure taps, 0·8 mm in diameter, were installed at regular intervals. The pressure taps were connected to the Scannivalve (48J9-1) and analog pressure signals were digitized using a high-precision A/D converter (DT 2838). At each channel, after 800 Hz low-pass filtering 40 960 pressure data were acquired at 2000 samples/s. A 10 s time delay was given to recover pressure fluctuations after each channel scanning.

The pressure difference between the surface pressure $P_s$ and the reference pressure $P_\infty$ measured at ambient free stream was nondimensionalized by the dynamic pressure with the free-stream velocity $U_0$. The pressure coefficient $C_p$ was expressed in the following form:

$$C_p = \frac{P_s - P_\infty}{\frac{1}{2}\rho U_0^2}.$$

The drag and lift forces acting on the cylinder were evaluated from the surface pressure distribution. If the contribution of skin friction on aerodynamic forces is negligibly small, the drag force can be represented by the form drag component. The drag coefficient, $C_D$, and lift coefficient, $C_L$, were obtained as follows:

$$C_D = \frac{D}{\frac{1}{2}\rho U_0^2 A_D}, \quad C_L = \frac{L}{\frac{1}{2}\rho U_0^2 A_L}.$$

Here, $A_D$ and $A_L$ are the frontal and projected areas of the cylinder.

Wake velocity profiles were measured using a hot-wire anemometer (TSI IFA 100) with I-type (DANTEC 55PI1) and X-type (DANTEC 55P61) probes. The X-type hot-wire probe was calibrated using the effective yaw calibration method and the effective yaw angle were $\Psi_1 = 44{\cdot}62^\circ$ and $\Psi_2 = 43{\cdot}61^\circ$. The hot-wire velocity signals were digitized at a sampling rate of 2000 Hz using the DT 2838 A/D converter. The hot-wire probes were traversed to the measuring positions using a 3-D traverse system having an accuracy of 0·01 mm. During experiments, the temperature variation in the wind tunnel test-section was maintained to be better than 0·5°C. Since the blockage ratio of the experimental model was less than 5%, the blockage effect was not corrected in this study.

The smoke-wire flow visualization technique was employed to visualize the gap effect on the flow interaction between the wake behind the elliptic cylinder and the flat plate boundary layer. A Nichrome wire, 0·1 mm in diameter, was installed vertically behind the elliptic cylinder. The smoke-wire was twisted and appropriate tension was given to the wire in order to compensate for its thermal expansion. The laser beam issuing from a Nd : YAG pulsed layer was passed through mirrors and a cylindrical lens to form a thin laser light sheet which illuminated the central streamwise section. Since the free-stream velocity was 2 m/s for this flow visualization, a trip wire of 7 mm diameter was used to make the same boundary layer thickness of 75 mm. Flow images were photographed using a still camera (Nikon F5) that was synchronized with the pulse laser and the electric power supplied to the smoke wire.

## 3. RESULTS AND DISCUSSION

### 3.1. Flow Visualization

Figure 2 shows flow visualization results for the elliptic cylinder of AR = 2 as a function of gap ratio ($G/B$). When the gap ratio is $G/B = 0{\cdot}2$, less than the critical value, we cannot see any vortices shed from the cylinder. On the other hand, when $G/B = 1{\cdot}0$, vortices are shed regularly and the vortex street is dominant in the downstream wake region as shown in Figure 2(c). For the gap ratio of $G/B = 0{\cdot}5$, the visualized flow reveals a combined effect of Figure 2(a) and 2(c). From this, we can guess that the critical gap ratio for the elliptic cylinder of AR = 2 exists around this value.

The extinction of regular vortex shedding can be explained by the following interference mechanism between the cylinder wake and the wall. The counterclockwise vortices in the lower side of the cylinder wake are mixed with opposite vortices of the boundary layer, and highly turbulent eddies appear intermittently in the outer layer of the turbulent boundary layer. These vortices and eddies penetrate into the wake region and weaken the vortex formation in the shear layer.

In addition, the flow on the flat plate was visualized using the ink dot method to see the extent of the recirculation region formed behind the cylinder which contacts with the plate ($G/B = 0$). For the elliptic cylinder of AR = 2, the recirculation region extends to the point of $X_R = 100$ mm at a free-stream velocity of $U_0 = 10$ m/s, which is half that of the circular cylinder ($X_R = 200$ mm).

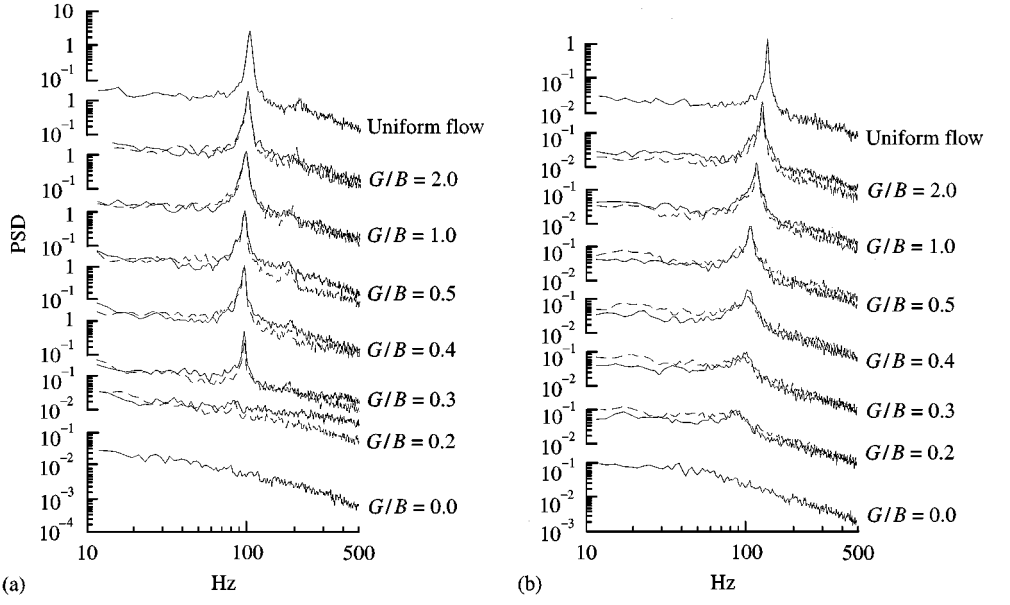


Figure 3 Power spectral density distributions at $x/A = 1{\cdot}0$: (a) AR = 1; (b) AR = 2; ——, $y/B = +0{\cdot}5$; – – –, $y/B = -0{\cdot}5$.

### 3.2. Critical Gap Ratio

In order to investigate the flow structure of the near wake behind the elliptic cylinder located near a flat plate, velocity fluctuations at various gap ratios were measured using a single hot-wire probe. For all velocity signals, spectral analysis was performed and the power spectral density (PSD) distributions at $x/A = 1{\cdot}0$ location are shown in Figure 3. When the cylinder is placed to touch the plate ($G/B = 0$), there is no clear peak on the PSD distribution. As the gap ratio ($G/B$) increases, a dominant peak begins to appear at the vortex-shedding frequency.

For the circular cylinder (AR = 1) having the same vertical height, we can see dominant peaks at both edges ($y/B = \pm 0{\cdot}5$) of the cylinder when the gap ratio is larger than $G/B = 0{\cdot}3$. This critical gap ratio is in agreement with that obtained by Bearman & Zdravkovich (1978), even though the boundary layer thickness is quite different. From this, we can see that the boundary layer thickness may be of little influence to the critical gap ratio. On the other hand, for the elliptic cylinder of AR = 2, a remarkable peak is observed for gap ratios larger than $G/B = 0{\cdot}4$. Therefore, the critical gap ratio of the elliptic cylinder, at which regular vortices start to be shed, is larger than that of the circular cylinder having the same blockage area.

The variations of the Strouhal number with respect to the gap ratio are presented in Figure 4. The Strouhal number, St, is defined as follows:

$$\mathrm{St} = \frac{Bf_s}{U_0},$$

where $f_s$ is the vortex-shedding frequency indicating the dominant peak in the PSD distribution.

For the circular cylinder (AR = 1), the Strouhal numbers measured at the upper and lower sides of the cylinder wake are identical and slowly increase as the gap ratio is

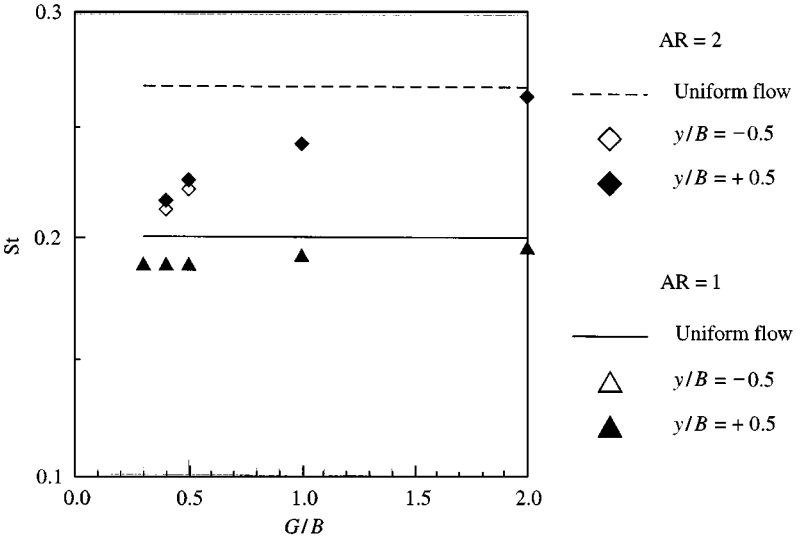


Figure 4. Variations of the Strouhal number, St, in terms of gap ratio, $G/B$.

increased. The maximum difference in the Strouhal number is about 6%. For comparison, the maximum variation of the Strouhal number obtained by Bearman & Zdravkovich (1978) was about 5%. The Strouhal number is nearly constant for gap ratios and almost independent of the thickness of the boundary layer. These results agree with those of Taniguchi & Miyakoshi (1990).

For the elliptic cylinder (AR = 2), however, the Strouhal numbers measured at the upper and lower sides of the cylinder wake are a little different at small gap ratios and abruptly decrease as the gap ratio is decreased. The variation of the Strouhal number with respect to the gap ratio reaches up to about 20%. These results reveal that the ground effect suppressing the vortex shedding appears strongly for the elliptic cylinder, compared to the circular cylinder.

### 3.3. Pressure Distribution

Figure 5 shows the pressure distributions on the cylinder surface as a function of gap ratio. For both the elliptic and circular cylinders, the surface pressure distributions becomesymmetric with respect to the cord of the cylinder as the gap ratio ($G/B$) increases. When the cylinder is placed in contact with the plate ($G/B = 0$), the pressure coefficient ($C_p$) on the lower surface has a nearly constant positive value on the front windward surface ($-0{\cdot}5 < x/A < 0{\cdot}0$) and a negative value on the leeward surface ($0{\cdot}0 < x/A < 0{\cdot}5$).

The pressure distributions on the circular cylinder (AR = 1) show a large deviation between the gap ratios of $G/B = 0{\cdot}2$ and $0{\cdot}5$. This result may be closely related to the critical gap ratio. For the elliptic cylinder of AR = 2, the effect of gap ratio on the surface pressure distributions is smaller than that for the circular cylinder, especially on the upper surface. For the gap ratios larger than $G/B = 0{\cdot}2$, the elliptic cylinder has higher $C_p$ value compared to the circular cylinder, on both the upper and lower surfaces. In the middle part of the upper surface, the surface pressure distributions do not change significantly, irrespective of the gap ratio, compared to the large discrepancy on the circular cylinder.

The variations of the base pressure, drag and lift coefficients acting on the cylinders are shown in Figure 6. The base pressure coefficient ($C_{PB}$) is defined as the pressure coefficient at

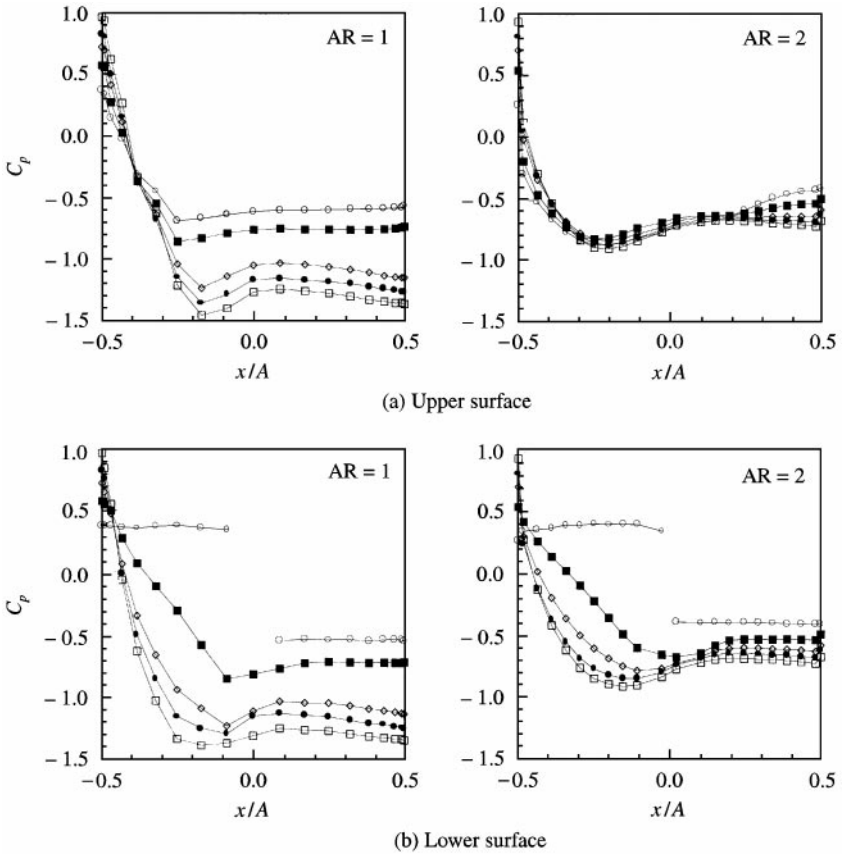


Figure 5. Surface pressure distributions for elliptic and circular cylinders: —○—, $G/B = 0$; —■—, $G/B = 0{\cdot}2$; —◇—, $G/B = 0{\cdot}5$; —●—, $G/B = 1{\cdot}0$; —□—, $G/B = 2{\cdot}0$.

the trailing edge of the cylinder. The base pressure of the elliptic cylinder is larger than that of the circular cylinder at all gap ratios tested. This results from the fact that the ground effect that suppresses the vortex shedding is larger and the velocity deficit in the wake centre is smaller compared to the circular cylinder, which is explained later.

For the circular cylinder (AR = 1), the base pressure is decreased rapidly as the gap ratio increases. The base pressure distributions show a large difference between $G/B = 0{\cdot}2$ and $G/B = 0{\cdot}5$ as shown in Figure 5; but above $G/B = 0{\cdot}5$, the base pressure decreases slowly with increasing gap ratio. This result is in good agreement with that of Bearman & Zdravkovich (1978). On the other hand, for the case of the elliptic cylinder (AR = 2), the base pressure decreases gradually as the gap ratio increases. Especially, the decrasing rate is much smaller than for a circular cylinder for small gap ratios less than $G/B = 0{\cdot}5$.

The drag coefficient estimated from the surface pressure data increases with increasing gap ratio. For small gap ratios less than $G/B = 0{\cdot}5$, the drag coefficient of the elliptic cylinder (AR = 2) increases slowly as the gap ratio increases. On the other hand, the drag coefficient of the circular cylinder increases rapidly. Here, it should be mentioned that the drag coefficient of the elliptic cylinder is about half that of the circular cylinder having the same height as the cylinder diameter. These drag coefficient curves closely correspond to the base pressure coefficient distributions shown in Figure 5.

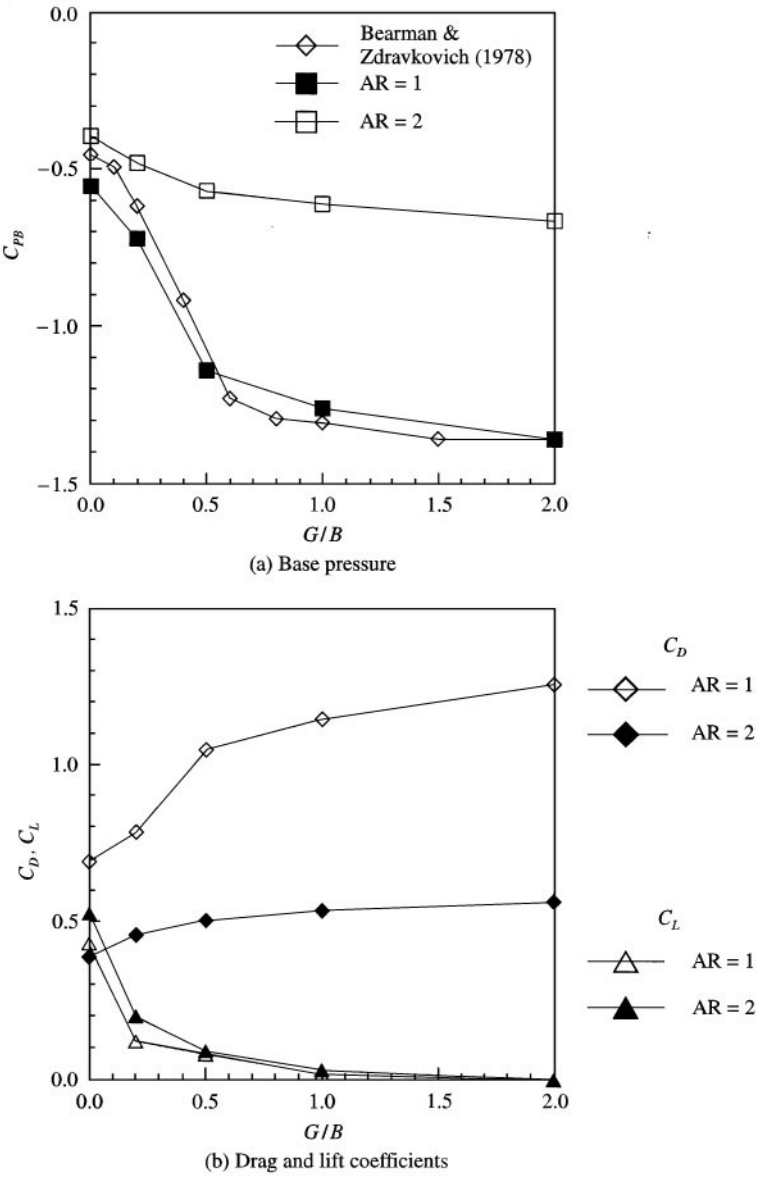


Figure 6. Variations of base pressure, drag and lift coefficients with $G/B$.

When the cylinder is placed in contact with the plate ($G/B = 0$), the cylinder has a positive lift coefficient. For gap ratios less than $G/B = 0{\cdot}5$, the elliptic cylinder has slightly higher lift coefficient than that of the circular cylinder. As the gap ratio increases, the lift coefficient decreases and converges to zero. This results from the fact that the surface pressure distributions become symmetric as the gap ratio increases.

The pressure distributions on the flat surface are shown in Figure 7 as a function of the gap ratio. When the cylinder contacts directly with the plate ($G/B = 0$), the pressure distribution has a discontinuity at the contact point; positive values on the front surface ($X/B < 0$) and negative values on the rear surface ($X/B > 0$). The negative pressure just behind the cylinder recover to the static pressure as the flow goes downstream. The location

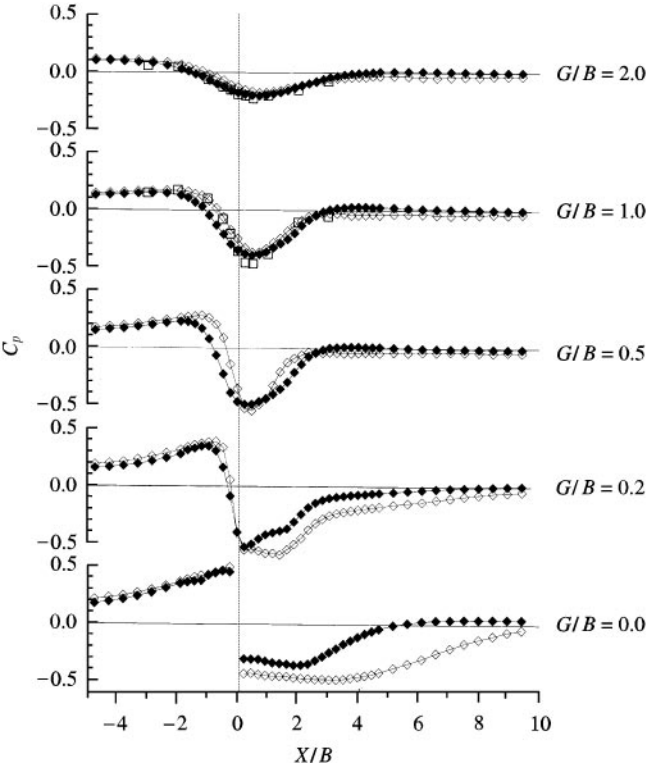


Figure 7. Surface pressure distributions on the flat plate: —◇—, AR = 1; —◆—, AR = 2; □, Bearman & Zdravkovich (1978).

from which the surface pressure starts to recover the static pressure value agrees with the reattachment point ($X_R$) of the recirculation region formed behind the cylinder. The surface pressures on the flat surface for the elliptic cylinder (AR = 2) are recovered faster than those of the circular cylinder, due to the smaller recirculation region.

On the front surface ($X/B < 0$), the maximum pressure occurs just in front of the contact point when the cylinder is in direct contact with the plate. With increasing gap ratio, the local maximum $C_p$ value is decreased and its location moves forward, regardless of the cylinder axis ratio. On the rear surface of the cylinder ($X/B > 0$), the surface pressure has a sharp negative peak just behind the centre location of the cylinder for the gap ratio of $G/B = 0{\cdot}2$. As the gap ratio increases, the minimum $C_p$ value is decreased and its location moves a little downstream. These gap flow effects on the surface pressure on the flat plate appear for all cases tested in this study, but are decreased as the gap ratio increases.

The geometric shape of cylinder has a large influence on the surface pressure distribution at smaller gap ratios. Especially, the elliptic cylinder having a slender-body shape has a much smaller surface pressure on the rear flat surface. The surface pressure results at large gap ratios for the case of circular cylinder are in good agreement with those of Bearman & Zdravkovich (1978), even though their boundary layer thicknesses are quite different.

### 3.4. Wake Velocity

Figure 8 shows the mean streamwise velocity profiles measured at $X = 100$, 150 and 200 mm locations. The solid line represents the velocity profile measured at the same

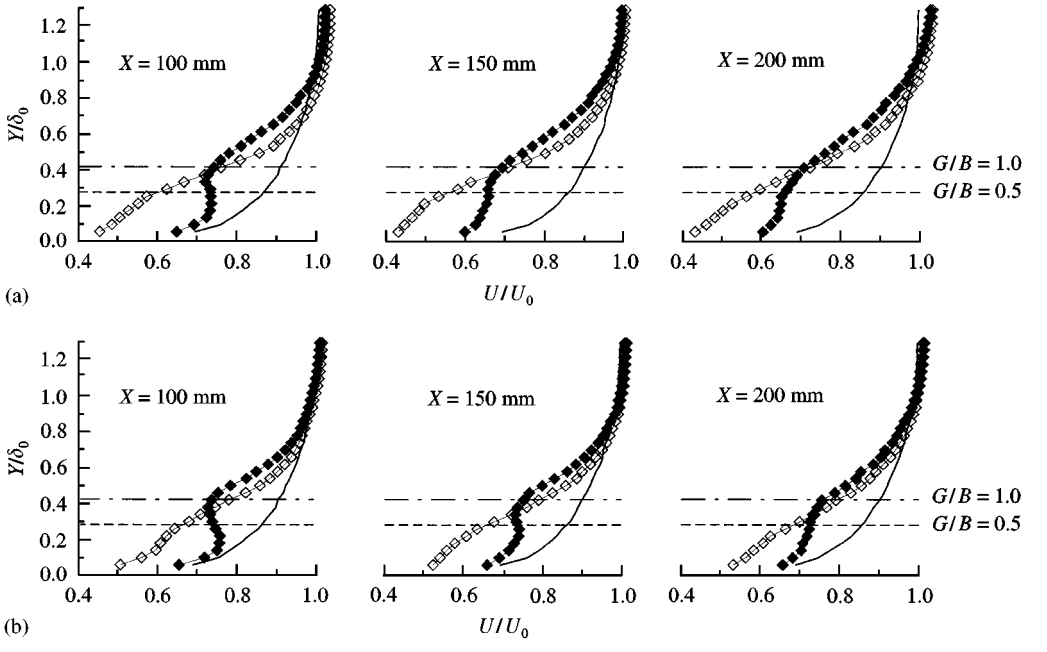


Figure 8. Mean streamwise velocity profiles at $X = 100$, 150 and 200 mm: (a) AR = 1; (b) AR = 2; ——, without cylinder; —◇—, $G/B = 0{\cdot}5$; —◆—, $G/B = 1{\cdot}0$.

location without the cylinder. The dashed and dash-dot-dash lines indicate the centre locations of the cylinder at $G/B = 0{\cdot}5$ and 1·0, respectively. The vertical length scale was nondimensionalized by the boundary layer thickness at $X = 0$ ($\delta_0 = 75$ mm).

Although the vortex shedding appears apparently in the near wake when the gap ratio is greater than 0·5, the wake structures for the gap ratios of $G/B = 0{\cdot}5$ and 1·0 are quite different from each other. For $G/B = 0{\cdot}5$, the mean streamwise velocity profiles have a similar profile at downstream locations, regardless of the cylinder axis ratio. At this gap ratio, the cylinder restricts the flow passing through the gap and serves to block the flow. Therefore, the streamwise velocity near the flat surface has a much smaller value than that at the gap ratio of $G/B = 1{\cdot}0$, irrespective of the axis ratio.

However, for the gap ratio of $G/B = 1{\cdot}0$, a velocity-deficit region is formed behind the cylinder and the streamwise velocity profiles near the wall become similar to the turbulent boundary layer due to the gap flow. However, as the flow goes downstream, the wake behind the circular cylinder is spread out toward the wall region. On the other hand, the wake behind the elliptic cylinder has less influence on the near-wall region compared to the circular cylinder. Therefore, the wake region formed inside the boundary layer is smaller than that of the circular cylinder.

The streamwise turbulence intensity profiles at $X = 100$, 150 and 200 mm are shown in Figure 9. The turbulence intensity profiles are quite different from those for the flat plate boundary layer without the cylinder, which is represented as a solid line. They have different shapes with respect to the gap ratio and the cylinder axis ratio. Especially, for the case of an elliptic cylinder, the clear double peaks do not appear, which is peculiar in the near wake behind a cylinder located in a uniform flow. In addition, the region having significant turbulent intensities due to the presence of the cylinder in the boundary layer is decreased, and the magnitude of the turbulent intensities is smaller compared to the case of the circular

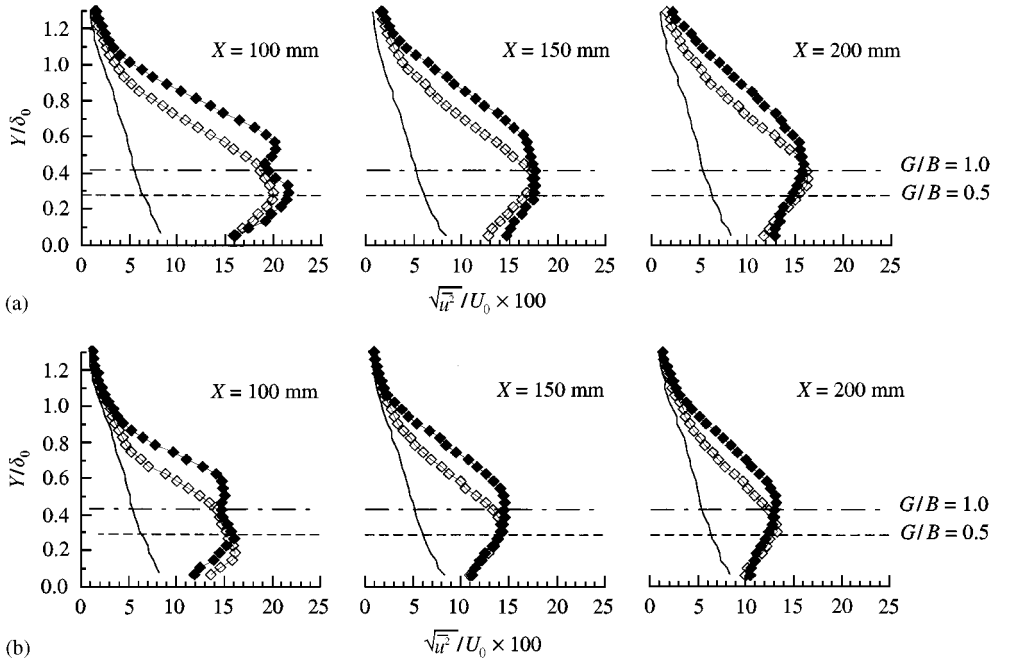


Figure 9. Streamwise turbulence intensity profiles at $X = 100$, 150 and 200 mm: (a) AR = 1; (b) AR = 2; ——, without cylinder; —◇—, $G/B = 0{\cdot}5$; —◆—, $G/B = 1{\cdot}0$.

cylinder. For the circular cylinder, however, the streamwise turbulent intensity profile at $X = 100$ mm shows the clear double peaks at $G/B = 1{\cdot}0$, even though the upper peak is a little smaller than the lower one. As the flow goes downstream, the double peaks disappear and merge to form a single peak.

In order to investigate the interaction between the cylinder wake and the turbulent boundary layer at downstream locations, a spectral analysis was performed for the vertical velocity component measured on the two sides ($y/B = \pm 0{\cdot}5$) of the cylinder wake. Figure 10 shows typical power spectral density distributions measured at $X = 100$ mm. When the gap ratio is $G/B = 0{\cdot}5$, the peak value of the power spectral density for the lower region ($y/B = -0{\cdot}5$) is smaller than that for the upper region, regardless of the cylinder axis ratio. Since the PSD results at the gap ratio of $G/B = 1{\cdot}0$ show a similar trend and the difference is not so large, we can conjecture that the vortex shedding on both sides of the cylinder occurs nearly at the same rate at $G/B = 1{\cdot}0$. From these results, we can evaluate that the ground effect on the cylinder wake constrains the shedding of vortices, especially in the lower side of the cylinder. In addition, the ground effect has a large influence on the wake of the elliptic cylinder, compared to that of the circular cylinder.

## 4. CONCLUSION

The ground effects on the flow characteristics around an elliptic cylinder located near a flat plate were investigated experimentally by varying the gap ratio ($G/B$) between the cylinder and plate. The elliptic cylinder having an axis ratio AR = 2 was embedded in a turbulent boundary layer whose thickness is larger than the height of the cylinder cross-section. For comparison, the same experiment was carried out for a circular cylinder having the same vertical height.

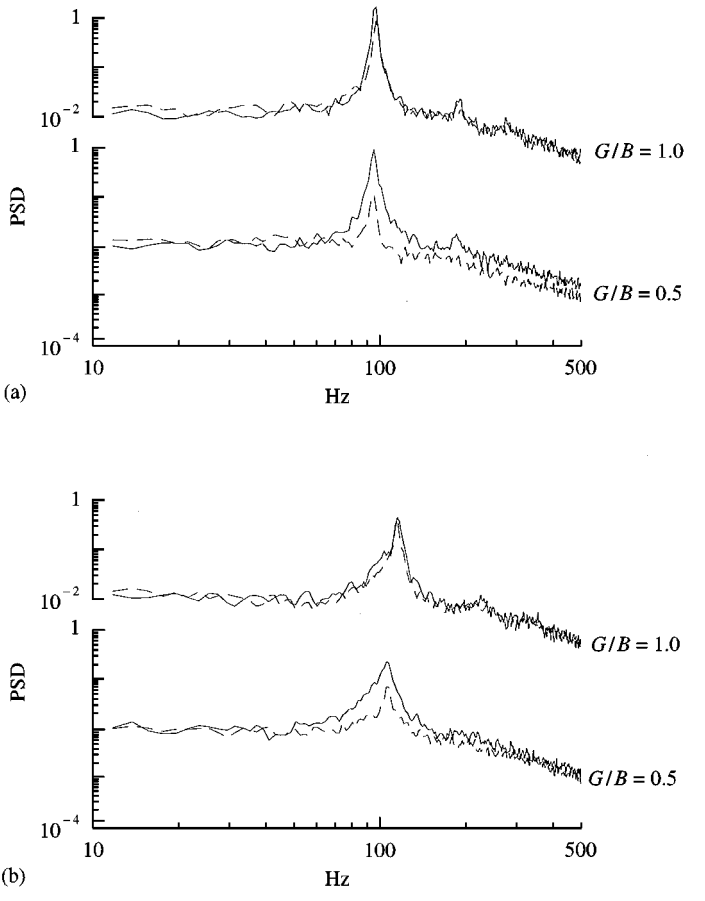


Figure 10. Power spectral density distributions of vertical velocity component measured at $X = 100$ mm: (a) AR = 1; (b) AR = 2; ——, $y/B = +0{\cdot}5$; – – –, $y/B = -0{\cdot}5$.

Regular vortex shedding occurs in the near wake when the gap ratio is greater than the critical value of $G/B = 0{\cdot}4$. The critical gap ratio is larger than that of a circular cylinder having the same vertical height. With decreasing gap ratio, the vortex-shedding frequency decreases abruptly for the case of the elliptic cylinder.

The deviation in surface pressure distribution on the elliptic cylinder with respect to the gap ratio is much smaller than that for the circular cylinder. This tendency is more dominant on the upper surface of the cylinder than on the lower surface. The surface pressures on the flat plate recover faster than for the circular cylinder at downstream locations.

As the gap ratio increases, the drag coefficient of the cylinder is increased, but the rate of increase is much smaller than for the circular cylinder at small gap ratios, less than $G/B = 0{\cdot}5$. The drag coefficient of the elliptic cylinder is about half that of the circular cylinder for all gap ratios tested in this study.

The ground effect on the cylinder wake constrains the shedding of vortices, especially more on the lower side of the cylinder wake than on the upper side. The wake region formed behind the elliptic cylinder and the turbulent intensities are much smaller than those of the circular cylinder.

## ACKNOWLEDGEMENT

This work was supported by AFERC (Advanced Fluids Engineering Research Center), POSTECH.

## References

ANGRILLI, F. & BERGAMASCHI, S. 1982 Investigation of wall induced modifications to vortex shedding from a circular cylinder. *Journal of Fluids Engineering* **104,** 518–522.

BEARMAN, P. W. & ZDRAVKOVICH, M. M. 1978 Flow around a circular cylinder near a plane boundary. *Journal of Fluid Mechanics* **89,** 33–47.

MARUMO, E., SUZUKI, K. & SATO, T. 1978 A turbulent boundary layer disturbed by a cylinder. *Journal of Fluid Mechanics* **87,** 121–141.

MODI, V. J. & DIKSHIT, A. K. 1975 Near wakes of elliptic cylinders in subcritical flow. *AIAA Journal* **13,** 490–497.

MODI, V. J. & WILAND, E. 1970 Unsteady aerodynamics of stationary elliptic cylinders in subcritical flow. *AIAA Journal* **8,** 1814–1821.

OTA, T., NISHIYAMA, H. & TAOKA, Y. 1984 Heat transfer and flow around an elliptic cylinder. *International Journal of Heat and Mass Transfer* **27,** 1771–1779.

OTA, T., NISHIYAMA, H. & TAOKA, Y. 1987 Flow around an elliptic cylinder in the critical Reynolds number regime. *Journal of Fluids Engineering* **109,** 149–155.

TANIGUGHI, S. & MIYAKOSHI, K. 1990 Fluctuating fluid forces acting on a circular cylinder and interference with a plane wall. *Experiments in Fluids* **9,** 197–204.

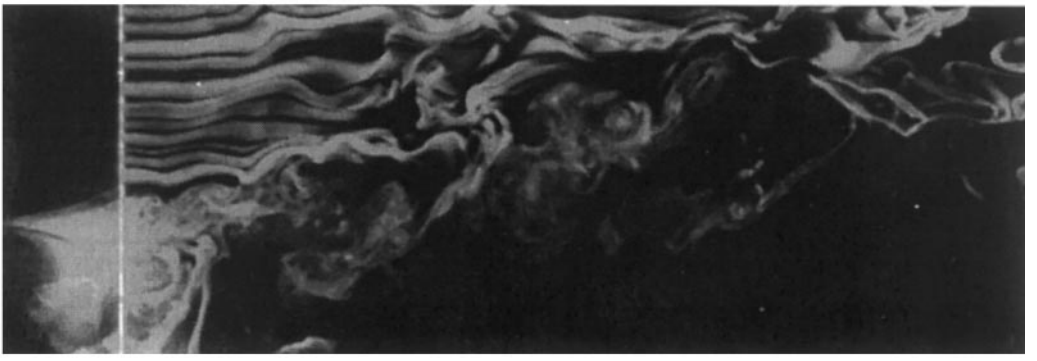

(a) $G/B = 0.2$

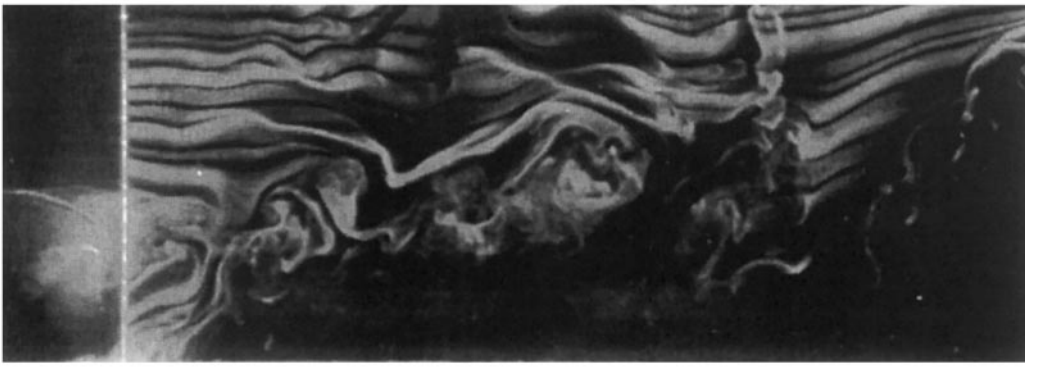

(b) $G/B = 0.5$

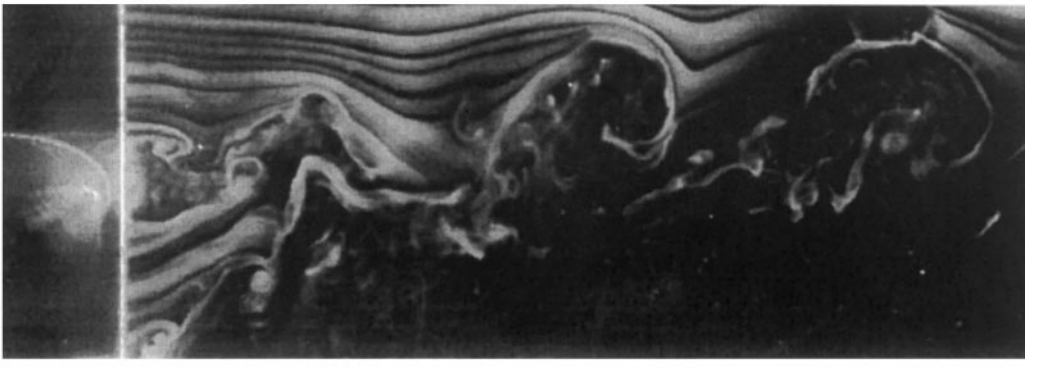

(c) $G/B = 1.0$

Figure 2. Flow visualization of the wake behind the elliptic cylinder (AR = 2) in terms of gap ratio $G/B$.